Evaluating simulated daily discharge for operational hydrological drought monitoring in the Global Drought Observatory (GDO)

C. Cammalleri , P. Barbosa & J. V. Vogt

Evaluating simulated daily discharge for operational hydrological drought monitoring in the Global Drought Observatory (GDO)

C. Cammalleri, P. Barbosa and J. V. Vogt

European Commission, Joint Research Centre (JRC), Ispra, Italy

ABSTRACT

Hydrological drought is currently underrepresented in global monitoring systems, mainly due the shortage of near real-time estimates of river discharge at the global scale. In this study, the outputs of the Lisflood model are used to define a low-flow drought index, which shows a good correspondence with long-term records of the Global Runoff Data Centre in the period 1980–2014, as well as with verified information from the literature on six major drought events (covering different regions and watershed sizes). In contrast, the near real-time simulation (from 2015 onward) provides temporally inconsistent estimates over about 20% of the modelled cells (mostly over South America and Central Africa), even if reasonable results are obtained over other regions, as confirmed by intercomparison with the operational outcomes of the European Drought Observatory for the 2018 drought. In spite of the highlighted limitations, valuable information for operational drought monitoring can be retrieved from these simulations.

1 Introduction

Drought is commonly seen as a "creeping" phenomenon, which develops slowly in time and impacts large areas both directly and indirectly. Contrary to common believe, drought can affect a variety of regions across the globe, and it is not limited to arid and semi-arid climates. Worldwide, around two billion people were affected and more than 10 million people died due to drought between 1900 and 2010 (van Loon 2015). In particular, hydrological drought can have severe impacts on ecological systems (e.g. Lake 2003), as well as on many economic sectors, including drinking water supply, crop production through irrigation and electricity production (see e.g. van Vliet *et al.* 2012, Wright *et al.* 2014, Madadgar *et al.* 2017).

Generally, hydrological drought is defined as a lack of water in the hydrological system, manifesting itself in abnormally low streamflow in rivers and/or levels in lakes, reservoirs and groundwater (Tallaksen and van Lanen 2004). Following this definition, it is clear that hydrological drought can be described through several variables, each one providing a different representation of the phenomenon. In the context of this study, streamflow is adopted as quantity for the monitoring of hydrological drought, thanks to its rapid response to meteorological drought compared to groundwater.

In more recent years, drought monitoring has gained a prominent role given the observed increases in frequency, duration and intensity of droughts and related impacts observed in the past decades (Trenberth *et al.* 2014, Spinoni *et al.* 2015). In response, several operational drought monitoring systems have been developed for various regions, ranging from a first approach to build a Global Drought Information System (GDIS)[1] covering the whole globe, to continental scale systems such as the US Drought Monitor,[2] the South Asia Drought Monitoring System (SADMS),[3] and the African Flood and Drought Monitoring (AFDM),[4] to the numerous national/regional systems.

At the European Commission, following the Communication to the European Parliament and the Council on "Addressing the challenge of water scarcity and droughts in the European Union" (EC, 2007), the Joint Research Centre (JRC) has developed various web-based platforms for the monitoring and forecasting of drought events from continental to global scale, including the European Drought Observatory (EDO)[5] and the Global Drought Observatory (GDO).[6] These systems comprise a set of multiple indicators aiming at covering the different facets of drought: meteorological drought indicators include the standardized precipitation index (SPI) and the standardized precipitation-evapotranspiration index (SPEI); agricultural drought is monitored through anomalies in soil moisture and the fraction of absorbed photosynthetically active radiation (fAPAR); and hydrological drought monitoring is behind in development, with a recently implemented low-flow index in EDO (Cammalleri *et al.*, 2017a).

Generally, most of the operational near real-time systems focus on meteorological and agricultural drought indicators,

[1]https://www.drought.gov/gdm/.
[2]http://droughtmonitor.unl.edu/.
[3]http://dms.iwmi.org/.
[4]http://stream.princeton.edu/AWCM/WEBPAGE/.
[5]http://edo.jrc.ec.europa.eu.
[6]http://edo.jrc.ec.europa.eu/gdo/.

especially at the largest spatial scales (i.e. global). This is likely due to the relative ease of retrieving rainfall, soil moisture or vegetation datasets (e.g. from remote sensing data). In fact, the major limitation for a global-scale hydrological drought monitoring is the lack of a reliable, self-consistent time series of water discharge data, delivered in near-real time and capable, on the one hand, of characterizing the typical low-flow regime of each river based on historical data and, on the other hand, of achieving timely detection of the start and the temporal evolution of a drought event.

Such characteristics can be achieved only by means of hydrological simulations, given the current sparseness of *in-situ* discharge measurements (Fekete and Vörösmarty 2007), but hydrological simulations are subject to uncertainties arising from various factors, principally in meteorological forcing and hydrological parameterization (Masaki *et al.* 2017). As an example, Müller Schmied *et al.* (2016) showed how different meteorological datasets derived from observations might affect simulated runoff and river discharge, highlighting the need of homogenized meteorological time series in practical applications. In addition, the availability of global near real-time meteorological datasets is quite limited, restraining the options for viable forcing.

A similar issue has been previously tackled in GDO for the soil moisture anomaly (SMA) indicator, where the final product combines Lisflood near real-time simulation of root-zone soil moisture with remote sensing proxies derived from the NASA MODIS (Moderate-resolution Imaging Spectroradiometer) land surface temperature and the ESA CCI (Climate Change Initiative) combined active/passive microwave product (Cammalleri *et al.* 2017b). In this operational product, the Lisflood model (see Section 2.1) is forced with daily meteorological maps derived from the European Centre for Medium-range Weather Forecasts (ECMWF) data, as spatially resampled and harmonized by the JRC Monitoring Agricultural ResourceS (MARS) group. Areas with inconsistent meteorological forcing were detected thanks to the cross-correlation with the two other products, whereas the use of anomalies limited the problem of absolute model calibration, since in this case relative temporal consistence becomes more important than absolute accuracy.

Starting from this experience, the same Lisflood near real-time simulation can be used to derive a low-flow drought index based on daily discharge simulations. However, even if Lisflood river discharge estimates are currently used for an operational forecast of flood events within the Global Flood Awareness System (GloFAS),[7] the suitability of such simulations for capturing the spatio-temporal dynamic of the low-flow regimes needs to be evaluated in detail. In addition, due to the absence of other products for a cross-validation of the outputs (similar to what was done for SMA by Cammalleri *et al.* 2017b), a key step of the analysis would be to evaluate the temporal consistency of the discharge time series in the most recent years compared to a consolidated historical dataset that has been validated against ground measurements from selected stations of the Global Runoff Data Centre (GRDC).[8]

Following these considerations, the main objective of this study is to investigate the feasibility of a near real-time monitoring of hydrological drought based on a low-flow index derived from daily river discharge maps, as simulated by the Lisflood model. To achieve this goal, both the historical baseline and the near real-time datasets were analysed in order to evaluate the joint capability of: (a) characterizing past drought events and low-flow regimes, and (b) capturing the start and severity of evolving drought events. The ultimate objective of the study is to provide insight into the implementation of such a low-flow indicator within the GDO operational monitoring system.

2 Materials and method

The proposed hydrological drought monitoring system is comprised of: (a) a near real-time simulation framework to monitor the daily evolution of river discharge, which also includes the characterization of the historical low-flow regimes, and (b) a statistically robust modelling framework to extrapolate a synthetic hydrological drought indicator from the combination of historical and near real-time daily discharge simulations. These two components are described in the next sub-sections, alongside the strategy adopted for the validation of the outcomes.

2.1 River discharge simulations

Daily river discharge data are simulated by means of the Lisflood distributed hydrological rainfall–runoff model (de Roo *et al.* 2000). The model simulates all the main hydrological processes occurring in the land–atmosphere system at grid-cell scale, including exchanges of evapotranspiration fluxes, infiltration, soil water redistribution in the vadose zone, surface runoff and groundwater dynamics (Burek *et al.* 2013). The surface runoff generated in each cell is channeled to the nearest river network cell by means of a routing component based on a four-point implicit finite-difference solution of the kinematic wave (Chow *et al.* 1988). This allows one to produce daily discharge maps covering the full river network.

The model set-up used is the one employed within GDO, including daily time-step simulations on a global regular grid of $0.1° \times 0.1°$. The river network is extracted from the high-resolution HydroSHEDS dataset (Lehner *et al.* 2008) and mapped at $0.1°$ using the scaling algorithm proposed by Fekete *et al.* (2001). More details on the characteristics of the operational model can be found in Alfieri *et al.* (2013), whereas specifics of the model calibration over 1287 stations through an evolutionary optimization algorithm, with the Kling-Gupta efficiency criterion (KGE) as objective function, are reported in Hirpa *et al.* (2018).

Model meteorological forcings were obtained from the JRC in-house MARS database, which harmonizes daily maps of precipitation, daily average temperature and three evapotranspiration products (from open water, from bare soil and from the reference crop) derived from the ECMWF simulations. In

---

[7]www.globalfloods.eu/.
[8]http://www.bafg.de.

this case, meteorological fields for the period 1980–2014 can be considered consolidated, whereas successive years were produced operationally in near-real time (with approx. 2 days of delay), as already used for the development of the SMA indicator in GDO.

2.2 Low-flow drought indicator

The hydrological drought index proposed herein is analogous to the low-flow indicator described in detail by Cammalleri *et al.* (2017a), who provide a validation over Europe and its operational implementation in EDO. The key quantity in this analysis is the total water deficit, computed from an unbroken sequence of discharge values below a defined low-flow threshold. More specifically, a daily changing threshold computed as the 95th percentile of a multi-year 31-day moving window is used. This approach helps to capture the seasonality that can be observed in the low-flow regimes in some climatological regions.

According to the theory of runs (Yevjevich 1967), a continuous period with discharge values below the defined low-flow threshold is considered as a drought event, whose severity is quantified by the total deficit (*D*, represented by the area enclosed by the threshold and the streamflow time series). To reduce the risk of including in the analysis small events without real impacts, two post-processing corrections are applied to the first-guess event dataset: (a) consecutive events with an inter-event interval smaller than 10 days are pooled together (Zelenhasić and Salvai 1987), and (b) small isolated events (of duration less than 5 days) are removed from the analysis (Jakubowski and Radczuk 2004). The first correction allows us to account for the statistical inter-dependency of events that are close in time, whereas the second reduces the effects of the uncertainty in the defined threshold by removing the events that have discharge values lower than the threshold only for a short period of time.

The set of water deficit values obtained for each cell from the historical time series (1980–2014) is used to derive the cumulative frequency of such events, which has been successively fitted to the Pareto Type II distribution (also known as Lomax distribution), formally expressed as:

$$F(D; \alpha; \lambda) = 1 - \left(1 + \frac{D}{\lambda}\right)^{-\alpha} \qquad (1)$$

where α and λ are the strictly positive shape and scale parameters, respectively, derived from the sample according to the maximum likelihood method. It is worth noticing that Cammalleri *et al.* (2017a) used the exponential distribution over the European domain, of which the Lomax can be considered a more general case since it is a special case of the generalized Pareto that is a mixture of the exponential and the gamma distributions. The choice of the Lomax distribution provides more flexibility to the fitting, in order to better adapt to a wider range of conditions and hydrological low-flow regimes that may be encountered at global scale compared to the European one.

Operationally, the fitting is performed only for the cells with more than five events within the 1980–2014 climatological dataset, as well as with a minimum contributing area of 1000 km² and a year-average streamflow greater than 10 m³ s⁻¹. The first constraint imposes a minimum standard in performing the fitting and evaluating its goodness, whereas the other two focus on removing from the analysis those secondary rivers or areas characterized by very limited flows.

The statistical goodness-of-fit is verified according to the Lilliefors test (1969), which requires a Monte Carlo estimation of the critical values of the Kolmogorov-Smirnov metric (for $p = 0.05$). This approach is suitable when the parameters are derived from the same sample, and a separation between calibration and validation sets is not possible due to the limited size of the sample.

2.3 Evaluation dataset

Since the Lisflood model has been developed primarily for the modelling of flood events, its capability to accurately characterize low streamflow conditions (i.e. drought) needs to be specifically evaluated. The capability to represent a low-flow regime can be quantified by comparing the modelled 95th percentile daily threshold (as defined in Section 2.2) against analogous limit values derived from ground measurements. With this aim, a set of discharge time-series was derived from the Global Runoff Data Centre (GRDC).[9] In particular, ground stations from the so-called "Climate Sensitive Dataset" were selected; this dataset includes almost 1200 stations respecting minimum criteria on temporal consistency, basin development, length of records and accuracy.

Among these stations, the ones respecting our imposed (more stringent) criteria on minimum upstream area (1000 km²) and average yearly flow (10 m³ s⁻¹), as well as a continuous coverage in the period 1980–2014, were extracted. Additionally, "duplicate" stations, located on the same river stretch or in nearby sub-basins, were removed in order to avoid overweighting the impact of these streams on the validation. As a result of this selection procedure, 80 stations were considered for the validation. It should be noted that this seemingly limited number of stations (compared to the original 1200) does not impact significantly on the spatial coverage of the original dataset, as can be seen in Fig. 2 by comparing the spatial distribution of the selected stations with the ones available in the GRDC web portal for the full dataset.[10]

In addition, the drought events derived from the historical dataset used to fit the Lomax distribution can be contrasted against recorded major past events. With this goal, a set of six well-documented drought events was selected, covering different regions of the globe, as well as different river size and flow values. The main characteristics of these six events are summarized in Table 1. All six events occurred during the period 1980–2014, with the oldest being the drought in California, USA, in the late 1980s/early 1990s, whereas the most recent one is the event in Kenya in the early 2010s.

---

[9]http://www.bafg.de.
[10]http://www.bafg.de/SharedDocs/Bilder/Bilder_GRDC/grdcTSEcss.jpg?__blob=poster.

Table 1. Summary of the drought events used to evaluate the baseline historical dataset.

Area	River	Avg. flow* ($m^3\ s^{-1}$)	Period	Peak year	Reference
California, USA	Sacramento	500	1987–1992	1991	State of California (2005)
Southeast Australia	Murray	370	2001–2009	2006	BoM (2007)
Yorkshire, UK	Derwent	90	1995–1997	1996	EDC (2013)
Balochistan/Sindh, Pakistan	Indus	2450	1998–2002	2000/01	Pakistan Weather Portal (2011)
Zona Sur, Chile	Bio-Bio	530	1996–1999	1998	Quintana (2000)
Kenya	Tana	50	2011–2012	2011	UN (2011)

*Values refer to the model cell used in the analysis (not necessarily the closing section of the basin); they are only indicative of the size of the river.

Finally, the near real-time component of the system was tested by evaluating the capability of the low-flow index to capture the spatio-temporal evolution of the recent well-documented drought event that occurred in central and northern Europe during the summer of 2018. During this event, the analogous low-flow index developed in EDO (Cammalleri *et al.*, 2017a) was already operationally implemented, by using a more reliable local meteorological dataset, providing a benchmark reference that can be used to investigate the soundness of the global low-flow indicator over this region.

The complete evaluation procedure, jointly with the various steps involved in the computation of the low-flow index, is summarized in the flow chart of Fig. 1, which highlights how the ground measurements, historical drought events and EDO maps are used to test the operational procedure in its various components.

3 Results and discussion

3.1 Test on the historical dataset

The 35-year historical dataset (1980–2014) was used to characterize the seasonality of the threshold used to define the upper boundary of the low-flow regime. To evaluate the capability of the Lisflood model to correctly reconstruct the observed dynamic, the same procedure was applied to measured river discharge data from the GRDC in order to obtain a benchmark dataset for comparison.

The maps in Fig. 2 show the Pearson correlation coefficient (r, Fig. 2(a)) and the Nash-Sutcliffe efficiency coefficient (E, Fig. 2(b)) for the 80 GRDC selected stations. Since the goal of this comparison is to evaluate the correspondence in low-flow dynamic, a preliminary bias correction of the data was performed, the aim being to focus only on the temporal dynamic without accounting for possible discrepancies in the magnitude of the two datasets.

The results reported in these maps (Fig. 2) highlight an overall good capability of Lisflood to capture the low-flow regime dynamic, with most of the values greater than 0.6 and 0.33 for r and E, respectively. This is better shown by the histograms depicted in Fig. 3, which highlight a rather negative skewed distribution for both r and E, with a median value of about 0.77 and 0.54, respectively. The fraction of values below the above reported threshold of 0.6 for r and 0.33 for E is 20% and 33%, respectively, with a very small fraction of data (less than 5% and 10% for r and E, respectively) lower than 0.

The spatial distribution of the values, as pictured in Fig. 2, shows a predominance of high values in South America and
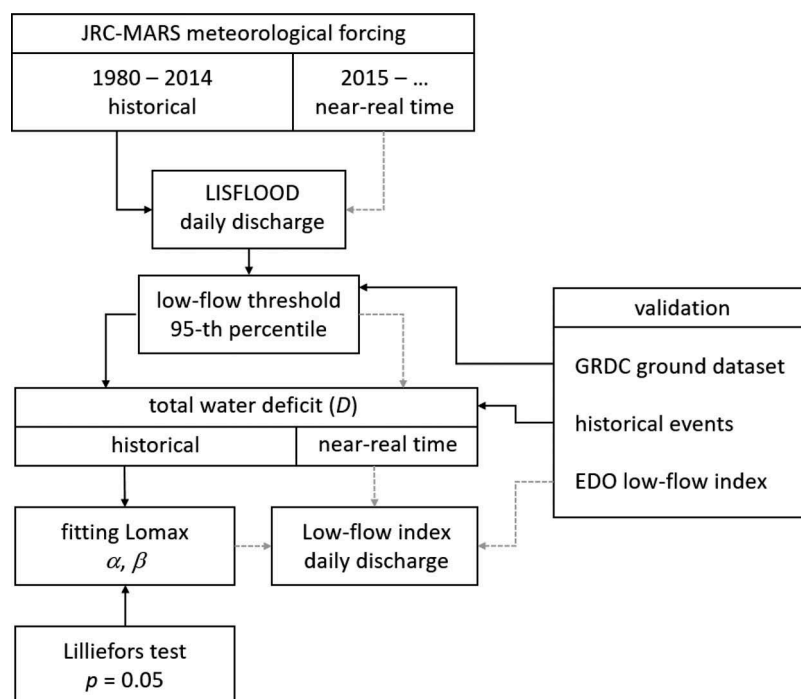

Figure 1. Flow chart describing the computation of the low-flow index, as well as the protocol adopted for the validation of the different steps of the operational procedure. Black lines represent operations on the historical data, whereas dashed grey lines represent operations on the near real-time data.
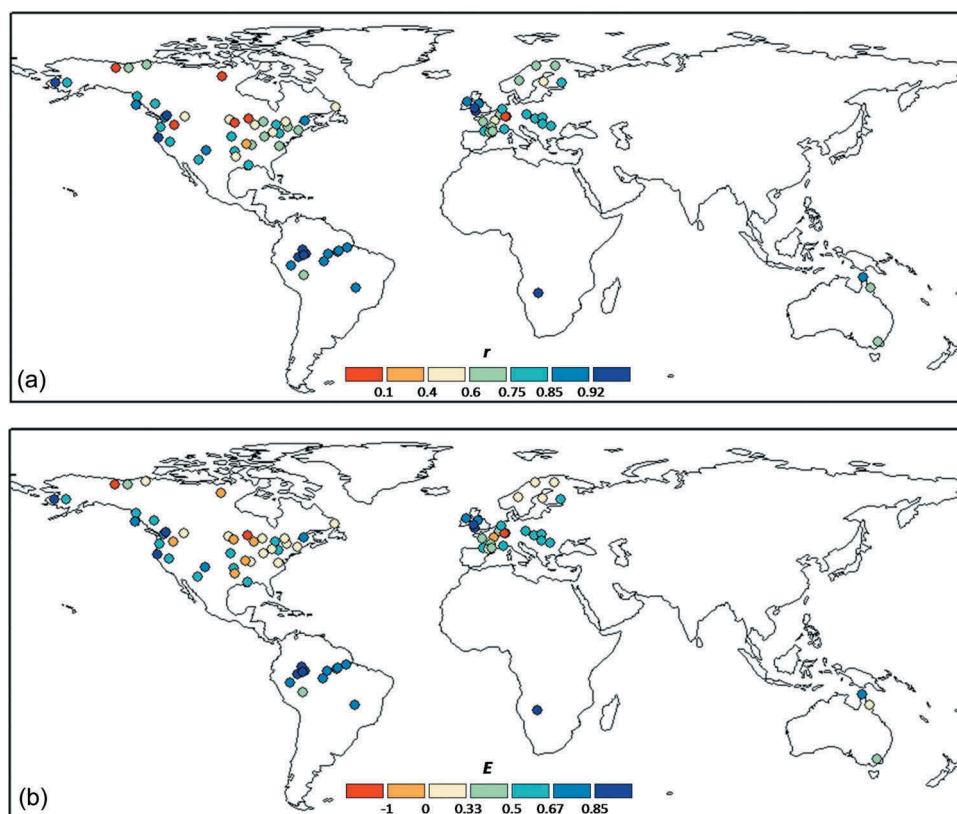
Figure 2. Spatial representation of (a) the Pearson correlation coefficient, *r*, and (b) the Nash-Sutcliffe efficiency coefficient, *E*, computed by comparing the low-flow threshold values (95th percentile) derived from the Lisflood historical simulation *vs* the GRDC ground stations.

Figure 3. Frequency distribution of (a) *r* values and (b) *E* values computed by comparing the low-flow threshold values (95th percentile) derived from the Lisflood historical simulation *vs* the GRDC ground stations.
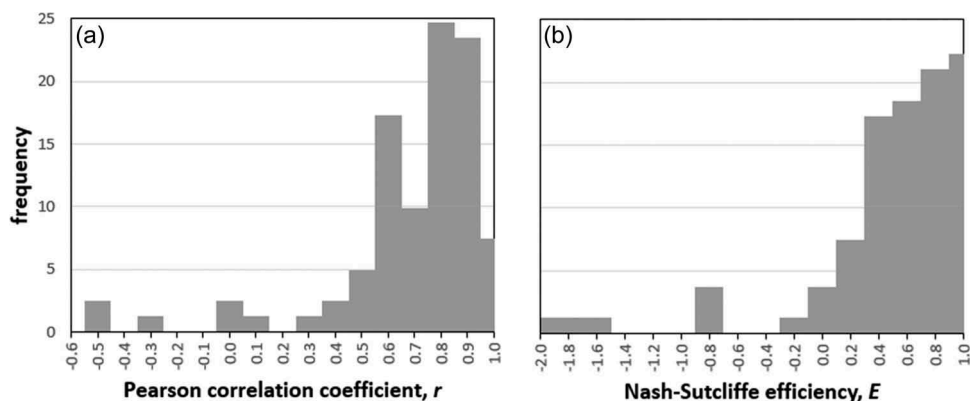
Europe, with some smaller values observed in central USA and Canada. Overall, the results suggest a substantial agreement with the observations, especially if the coarse resolution of the modelled data (0.1°) and the focus only on the low-flow regime are considered. At the same time, we have to note that the lack of ground measurements in Africa, Asia and large parts of Australia results in uncertainties for the modelling accuracy in those parts of the globe.

The modelled threshold values were used within the theory of runs to define a dataset of drought events for each grid cell, whose empirical frequency distribution was fitted with the Lomax distribution. The goodness of fit was tested for all the cells with at least: (a) more than 5 events, (b) a minimum

contributing area of 1000 km^2 and (c) a year-average streamflow greater than 10 m^3 s^{-1} (corresponding to 187 700 grid cells). The outcome of the Lilliefors test highlights a statistically significant fitting ($p = 0.05$) for about 96% of the cells, with a spatial distribution of the corresponding p values as depicted in Fig. 4 (only the cells with at least 10 000 km^2 of drainage area are reported in the map to improve the legibility). Figure 4 further highlights the overall good performance of the Lomax distribution in capturing the statistical structure of the historical drought events, with a small concentration of non-significant fittings concentrated in the Middle East; this behavior may be partially related to the frequent dry conditions experienced in those regions, which may not be well captured by the chosen
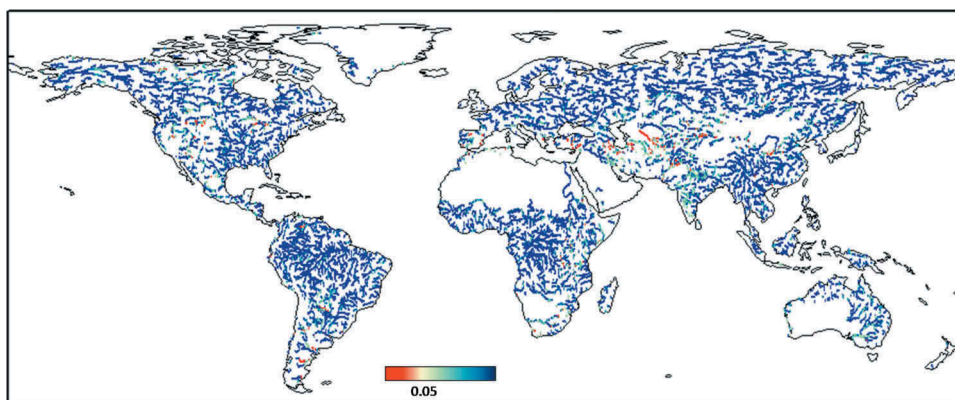
Figure 4. Spatial distribution of the *p* values obtained according to the Lilliefors test procedure. For the sake of clarity, only the data for the grid cells with at least 10 000 km² drainage area are reported.

probability distribution. Overall, the obtained fittings seem suitable for operational use in the context of a drought monitoring system.

The capability of this historical dataset to capture the actual dynamic of past droughts is evaluated qualitatively for the six case studies summarized in Table 1. With this aim, all the deficit periods retrieved by the model in the same year were summed-up and plotted in Fig. 5, with the goal to easily highlight the years that had prolonged low-flow periods according to our proposed indicator. Contextually, the years classified as under drought according to the sources reported in Table 1 are demarked by the grey-filled areas in the plots. Additionally, under each plot, a detailed evolution of the monthly values of the low-flow indicator is depicted for the 3 years across the drought peak. In these time-series, the $F_{(D)}$ values were classified according to the colour code currently in use in EDO, as: mild ($0 < F_{(D)} \le 0.25$, yellow), moderate ($0.25 < F_{(D)} \le 0.5$, orange), severe ($0.5 < F_{(D)} \le 0.75$, red) and extreme ($F_{(D)} > 0.75$, maroon).

A first analysis of the yearly time series in Fig. 5 highlights how the years affected by significant drought can be clearly seen in comparison to the rest of the historical period in all cases, suggesting a good capability of the model to discriminate between drought and regular years. Additionally, by comparing the plots with the values reported in Table 1, it is possible to observe a good correspondence between the major modelled events and the peak years, with the only exception of the Indus River for which the modelled event seems to occur slightly later than the observed one. It is worth noticing that the weaker events of 2005 and 2009 can be also correctly observed over this area.

According to the max $F_{(D)}$ value retrieved for each major event during the peak year, it seems that all the case studies can be classified as extreme, which is accurate given the well-known relevancy of such events. Overall, despite being limited to a few major past drought events, this analysis seems to support the capability of the model to capture both the timing and the severity of these events, with no clear discrepancies, either between small and large rivers or along the time series.

3.2 Near real-time application

Temporal inconsistencies can arise when the threshold values derived from an historical dataset are mixed with the near real-time estimates of river discharge. This can be especially true over areas where the meteorological forcing is less reliable, which can lead to biased estimates of the low-flow indicator. In order to demark those areas, an analysis on the annual minimal flow was performed, by detecting through the Welch *t* test (Welch 1947) the cells in which the key statistics (average and standard deviation) for the period 1980–2014 significantly differ (at $p = 0.01$) from those for the period 2015–2018.

This test detected statistically significant differences for about 20% of the modelling cells, mainly those located in Central Africa and South America (Fig. 6). Both areas are among the prominent ones where Lisflood soil moisture anomalies had a low correlation with the two remote sensing products used in Cammalleri *et al.* (2017b), confirming the need to improve model quality over those regions (see Fig. 1 of Cammalleri *et al.* 2017b for comparison). This result highlights the likely difficulties in correctly detecting hydrological drought events in a near real-time framework over these regions in the most recent years, suggesting the need to mask-out these cells in the case of operational monitoring.

To test the reliability of a masking procedure based on the outcomes of the Welch *t* test, the $F_{(D)}$ indicator was computed on 10-day periods (dekads, corresponding to three periods per month) and the fraction of dekads with $F_{(D)} > 0.25$ (i.e. at least moderate drought) in a 5-year window was computed. Figure 7 reports the number of cells corresponding to a certain fraction value, depicting the results for all the 5-year periods preceding 2015 (1980–1984, 1985–1989, … in grey), as well as the most recent 5-year window (2015–2019) before (continuous black line) and after (dotted black line) the masking.

These results show that the period 2015–2019 falls in line with the previous years only once the masking is applied, highlighting an unusually high number of cells with very long periods of drought (>30% of the total time) before the masking. Even if the masking procedure seems overall successful in removing unreliable outcomes, it is still possible to notice some residual errors in the analysis, with a slightly higher number of cells with more than one-third of the dekads in the period under at least a moderate drought, even after the correction. However, this number is significantly reduced when compared to the unrealistic one observed before the masking was applied.
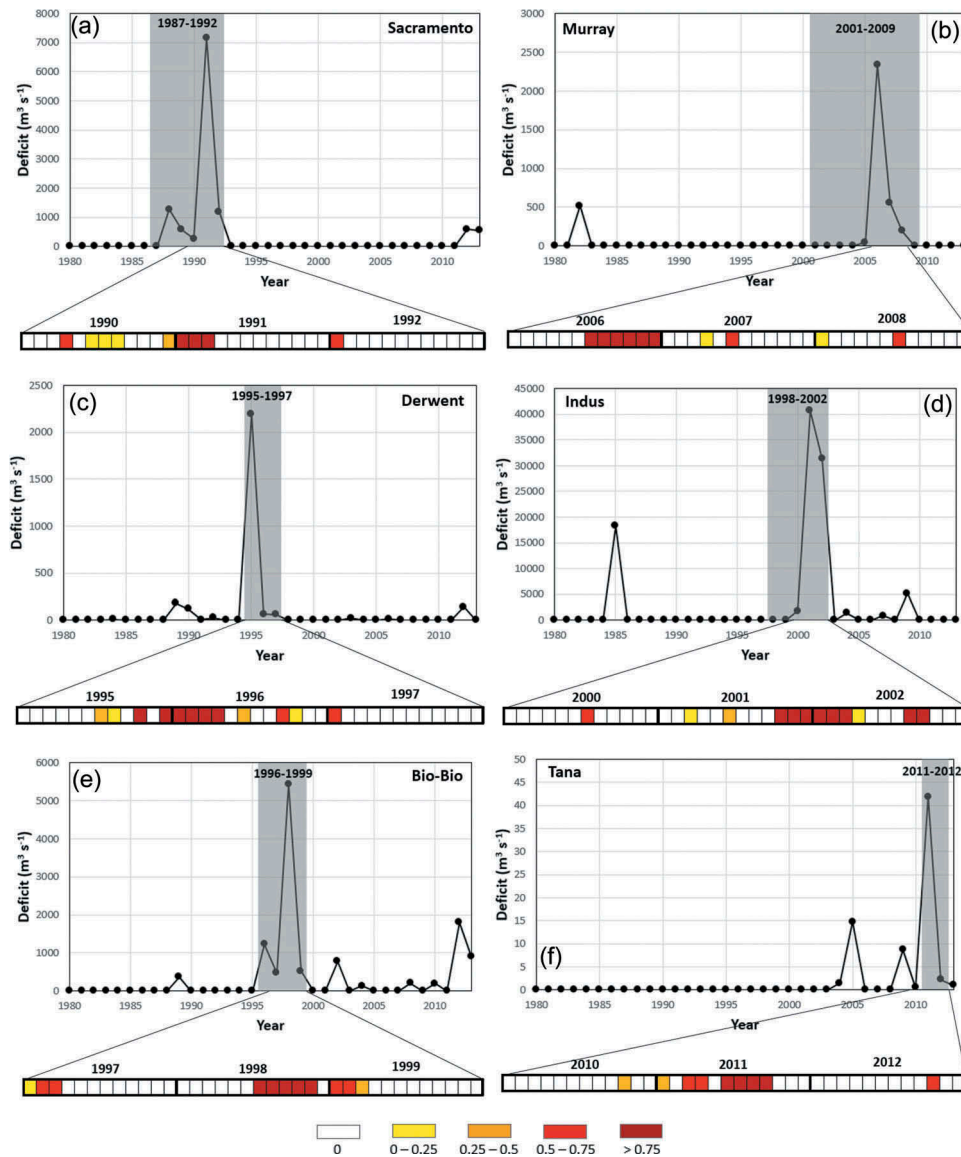
Figure 5. Total deficit values obtained from the historical dataset for the six selected test cases. The main panels show the year-total deficit, whereas the lower bars report the monthly details for the specific drought years. The colour scheme adopted here is analogous to the one used in Cammalleri *et al.* (2017a): mild: yellow, moderate: orange, severe: red, extreme, maroon.
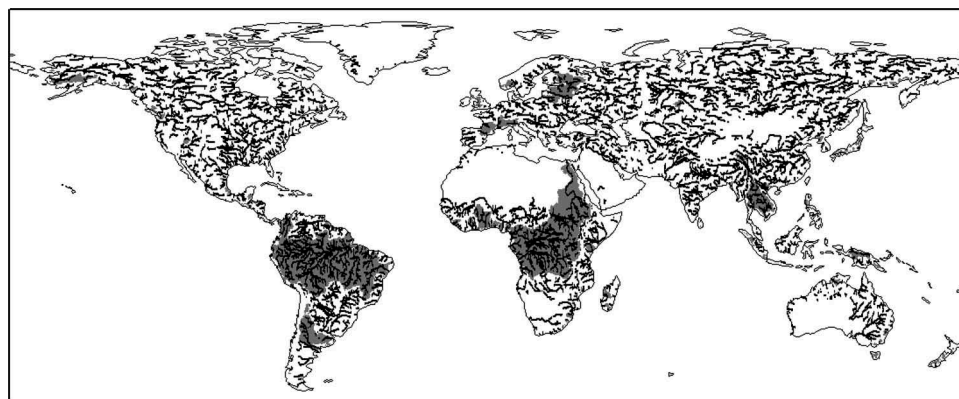

Figure 6. Water basins (grey shaded areas) where the Welch *t* test detects statistically significant differences between historical (1980–2014) and near real-time (2015–2018) annual minimum discharge.
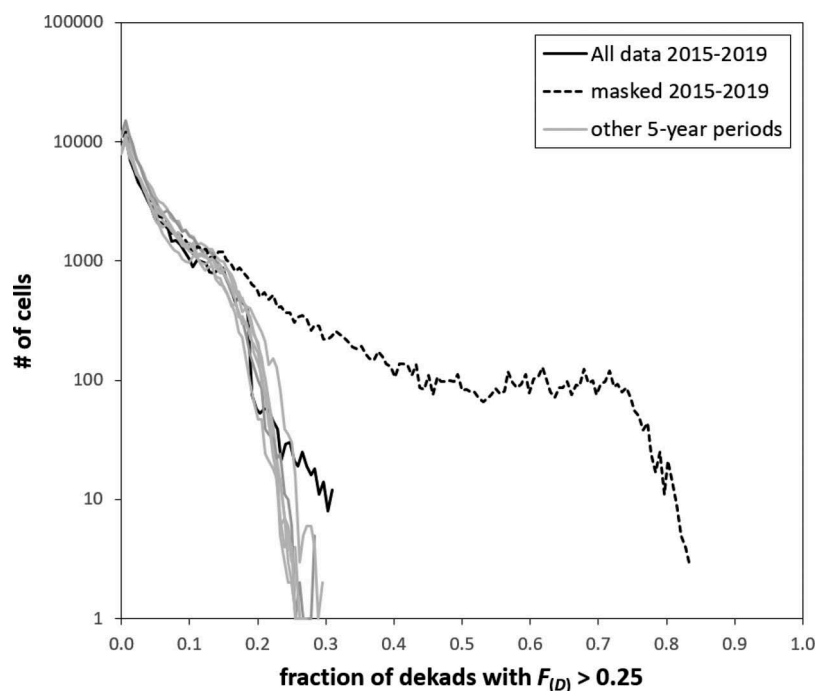
Figure 7. Number of cells (in logarithmic scale) having a certain fraction of all the 10-day periods (dekads) in a 5-year window under at least moderate drought conditions ($F_{(D)} > 0.25$). As an example, a value of 0.1 corresponds to a cell with 18 dekads (out of the 180 in 5 years) with $F_{(D)} > 0.25$. The grey lines represent all the 5-year periods before 2015, whereas the continuous and dotted black lines represent the period 2015–2019 before and after the masking, respectively.

As a final test of the near real-time product, the dekadal $F_{(D)}$ maps produced by the "simulated" operational global model (namely sim-GDO) were compared against those already available operationally in the EDO system (namely ope-EDO). In particular, four maps extracted from the full time series were selected to highlight the key phases of the drought event affecting Europe during the second half of 2018, as reported in Fig. 8 for both ope-EDO (left) and sim-GDO (right).

The time series of ope-EDO maps (Fig. 8, left) shows the first signs of drought at the beginning of June, which already quickly develop into severe conditions over most of the southern Scandinavian Peninsula in July. Consequently, the drought migrated to the south, covering most of central Europe (most notably Germany) at the beginning of December, before disappearing almost completely around January 2019. Overall, the sim-GDO times series (right) seems able to capture the evolution of the event in both its temporal and spatial main traits, even if it is possible to notice a tendency to underestimate the extent of the area affected in central Europe (i.e. map for the first dekad of December). In spite of these discrepancies, the intercomparison highlights a good consistency between the two products, suggesting a possible successful implementation of the indicator within the global drought monitoring system, given the limitations already discussed.

4 Summary and conclusions

To date, applications of hydrological drought indicators for a near real-time hydrological drought monitoring, specifically the ones based on low-flow conditions in river discharge, have been limited compared to meteorological and agricultural drought. This is mainly due to the strong dependency on global runs of hydrological models, whose feasibility is still limited by data availability for both model calibration and forcing. Starting from the Lisflood simulations produced operationally for the soil moisture anomaly (SMA) indicator, available in the Global Drought Observatory (GDO), the goal of this study was to evaluate the viability of monitoring hydrological droughts at the global scale based on simulated daily river discharge maps.

The two main constraints for such an application are: first, the reliability of the low flow regimes simulated by a model specifically designed for flood detection and, second, the temporal consistency of the discharge time series based on the combination of historical and near real-time data. The comparison with ground data, even if these are limited in spatial coverage, confirms the good capability of the model to capture low-flow regimes under various conditions, despite its origin as a flood forecasting model. This allows past drought events (between 1980 and 2014) to be fitted with the Lomax probability distribution. This modelling framework proved to be well suited to capture the probabilistic characteristics of hydrological drought events across the globe, with about 96% of the cells reporting a statistically significant fitting ($p = 0.05$).

The historical simulation demonstrated the ability to satisfactorily capture the temporal dynamic of six historical cases, which were selected as benchmark cases covering a wide range of conditions. However, the Welch t test analysis (focusing on the temporal consistency between the historical and recent simulations) highlighted the large uncertainties in monitoring hydrological droughts over certain regions of the world with the current model set-up (about 20% of the domain, most notably over South America and Central Africa).
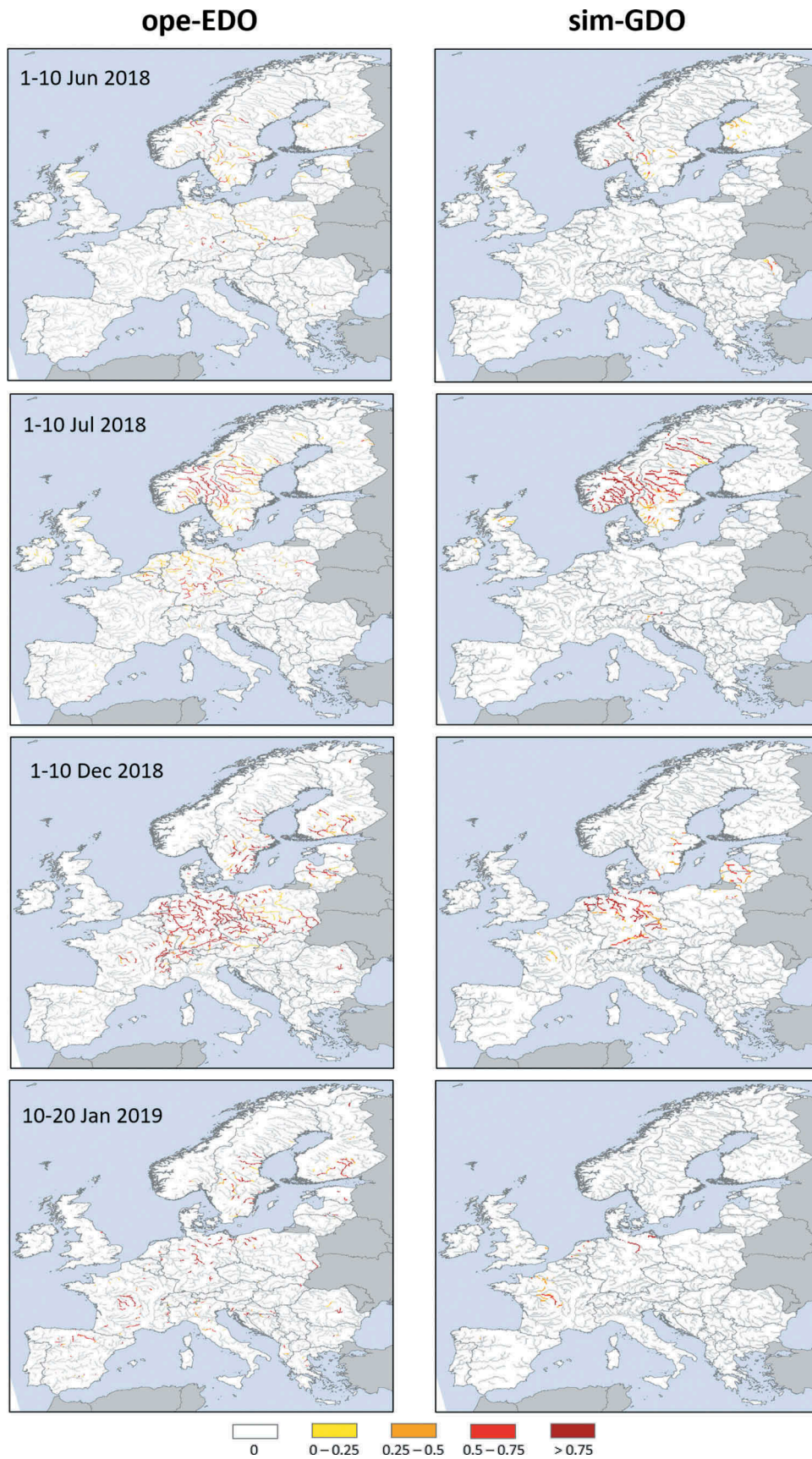
Figure 8. Spatio-temporal evolution of the European drought during the second half of 2018. Maps on the left are derived from the operational EDO system (ope-EDO), whereas maps on right simulate the outcome of a future analogous product in the GDO system (sim-GDO).

The additional comparison of the global dataset with the already implemented operational system in EDO showed good consistency in both the temporal and spatial traits of the European drought of 2018. This outcome confirms the reliability of the estimates of the global model over areas where no significant temporal inconsistency in the times series is detected by the Welch t test.

The results reported in this study highlight the boundary of what is currently achievable with the analysed combination of model and forcing in an operational setting, emphasizing the main spatial limitations of a potential future implementation in GDO. In spite of these limitations, the inclusion of a Lisflood-based low-flow indicator in GDO will represent a first step in the operational monitoring of hydrological drought at the global scale. It will fill the gap in the current global monitoring system, and potentially lead to further improvements of the system based on the performance of this operational index in the case of future drought events.

Disclosure statement

References

Alfieri, L., *et al.*, 2013. GloFAS – global ensemble streamflow forecasting and flood early warning. *Hydrology and Earth System Sciences*, 17 (3), 1161–1175. doi:10.5194/hess-17-1161-2013

BoM (Bureau of Meteorology, Australia), 2007. *Annual Australian climate statement 2006: a year of climate contrasts* [online]. Available from: http://www.bom.gov.au/announcements/media_releases/climate/change/20070103.shtml [Accessed 5 April 2018].

Burek, P., van der Knijff, J.M., and de Roo, A., 2013. *LISFLOOD: distributed water balance and flood simulation model*. JRC Scientific and Technical Reports, EUR 26162 EN, 142 pp. doi:10.2788/24719.

Cammalleri, C., *et al.*, 2017b. Comparing soil moisture anomalies from multiple independent sources over different regions across the globe. *Hydrology and Earth System Sciences*, 21 (12), 6329–6343. doi:10.5194/hess-21-6329-2017

Cammalleri, C., Vogt, J., and Salamon, P., 2017a. Development of an operational low-flow index for hydrological drought monitoring over Europe. *Hydrological Sciences Journal*, 62 (3), 346–358.

Chow, V.T., Maidment, D., and Mays, L.W., 1988. *Applied Hydrology*. New York: McGraw-Hill.

de Roo, A., Wesseling, C., and van Deusen, W., 2000. Physically based river basin modelling within a GIS: the LISFLOOD model. *Hydrological Processes*, 14 (11–12), 1981–1992. doi:10.1002/()1099-1085

EC (European Commission), 2007. *Communication from the commission to the European Parliament and council: addressing the challenge of water scarcity and droughts in the European Union*. COM(2007) 414 final. Available from: http://eur-lex.europa.eu/LexUriServ/LexUriServ.do?uri=COM:2012:0673:FIN:EN:PDF [Accessed 13 March 2020].

EDC (European Drought Centre), 2013. *Drought of 1995–1996: northern Europe* [online]. European Drought Reference and European Drought Impact Report Inventory. Available from: http://www.geo.uio.no/edc/droughtdb/edr/DroughtEvents/1996_Event.php [Accessed 5 April 2018].

Fekete, B.M. and Vörösmarty, C.J., 2007. The current status of global river discharge monitoring and potential new technologies complementing traditional discharge measurements. *In*: *Predictions in ungauged basins: PUB kick-off*. vol. 309. Wallingford, UK: IAHS Press, 129–136.

Fekete, B.M., Vörösmarty, C.J., and lammers, R.B., 2001. Scaling gridded river networks for macroscale hydrology: development, analysis, and control of error. *Water Resources Research*, 37 (7), 1955–1967. doi:10.1029/2001WR900024

Hirpa, F.A., *et al.*, 2018. Calibration of the Global Flood Awareness System (GloFAS) using daily streamflow data. *Journal of Hydrology*, 566, 595–606. doi:10.1016/j.jhydrol.2018.09.052

Jakubowski, W. and Radczuk, L., 2004. Estimation of hydrological drought characteristics NIZOWKA2003 – software Manual. *In*: L. M. Tallaksen and H.A.J. van Lanen, eds. *Hydrological drought – processes and estimation methods for streamflow and groundwater*. Amsterdam, The Netherlands: Elsevier Science BV [CD-ROM].

Lake, P.S., 2003. Ecological effects of perturbation by drought in flowing waters. *Freshwater Biology*, 48 (7), 1161–1172. doi:10.1046/j.1365-2427.2003.01086.x

Lehner, B., Verdin, K., and Jarvis, A., 2008. New global hydrography derived from spaceborne elevation data. *Eos, Transactions of the American Geophysical Union*, 89 (10), 93–94. doi:10.1029/2008EO100001

Lilliefors, H.W., 1969. On the Kolmogorov-Smirnov test on the exponential distribution with mean unknown. *Journal of the American Statistical Association*, 64, 387–389. doi:10.1080/01621459.1969.10500983

Madadgar, S., *et al.*, 2017. Probabilistic estimates of drought impacts on agricultural production. *Geophysical Research Letters*, 44 (15), 7799–7807. doi:10.1002/2017GL073606

Masaki, Y., *et al.*, 2017. Intercomparison of global river discharge simulations focusing on dam operation-multiple models analysis in two case-study river basins, Missouri-Mississippi and Green-Colorado. *Envonmental Research Letters*, 12 (5), 055002. doi:10.1088/1748-9326/aa57a8

Müller Schmied, H., *et al.*, 2016. Variations of global and continental water balance components as impacted by climate forcing uncertainty and human water use. *Hydrology and Earth System Sciences*, 20 (7), 2877–2898. doi:10.5194/hess-20-2877-2016

Pakistan Weather Portal, 2011. *History of drought in Pakistan – in detail* [online]. Available from: https://pakistanweatherportal.com/2011/05/08/history-of-drought-in-pakistan-in-detail/ [Accessed 5 April 2018].

Quintana, J., 2000. The drought in Chile and La Niña. *Drought Network News*, 12 (2), 1–6.

Spinoni, J., *et al.*, 2015. European drought climatologies and trends based on a multi-indicator approach. *Global and Planetary Change*, 127, 50–57. doi:10.1016/j.gloplacha.2015.01.012

State of California, 2005. *California's most significant droughts: comparing historical and recent conditions* [online]. Available from: https://www.water.ca.gov/LegacyFiles/waterconditions/docs/California_Signficant_Droughts_2015_small.pdf [Accessed 5 April 2018].

Tallaksen, L.M. and van Lanen, H.A.J., 2004. *Hydrological drought: processes and estimation methods for streamflow and groundwater. I*Developments in water science series, vol. 48. Amsterdam, The Netherlands: Elsevier Science BV.

Trenberth, K.E., *et al.*, 2014. Global warming and changes in drought. *Nature Climate Change*, 4 (1), 17–22. doi:10.1038/nclimate2067

UN (United Nations), 2011. *Humanitarian requirements for the Horn of Africa drought* [online]. Available from: https://reliefweb.int/sites/reliefweb.int/files/resources/Full_report_216.pdf [Accessed 5 April 2018].

van Loon, A.F., 2015. Hydrological drought explained. *WIREs Water*, 2 (4), 359–392. doi:10.1002/wat2.1085

van Vliet, M.T.H., *et al.*, 2012. Vulnerability of US and European electricity supply to climate change. *Nature Climate Change*, 2 (9), 676–681. doi:10.1038/nclimate1546

Welch, B.L., 1947. The generalization of "Student's" problem when several different population variances are involved. *Biometrika*, 34 (1–2), 28–35. doi:10.1093/biomet/34.1-2.28

Wright, B., *et al.*, 2014. Managing water quality impacts from drought on drinking water supplies. *Journal of Water Supply Research and Technology*, 63 (3), 179–188. doi:10.2166/aqua.2013.123

Yevjevich, V., 1967. *An objective approach to definitions and investigations of continental hydrological droughts*. Fort Collins, CO: Colorado State University, Hydrology Paper 23.

Zelenhasić, E. and Salvai, A., 1987. A method of streamflow drought analysis. *Water Resources Research*, 23 (1), 156–168. doi:10.1029/WR023i001p00156